ORIGINAL PAPER

Photoluminescent and multi-phonon resonance Raman scattering dual-mode immunoassays based on CdS nanoparticles for HIgG detection

Hongyi Li[1] · Xiaokun Wen[1] · Yadan Ding[1] · Guorui Wang[1] · Hancheng Zhu[1] · Junping Liu[1] · Huiying Zhao[2] · Xia Hong[1]

Abstract

A dual-mode immunoassay strategy based on CdS nanoparticles as signal probes with both of photoluminescent (PL) and multi-phonon resonance Raman scattering (MRRS) properties was developed. Simplified structural design and preparation were achieved due to the intrinsic integration of PL and MRRS dual signals in the single-unit CdS nanoprobes. Human immunoglobulin G (HIgG) was sensitively and specifically detected using the proposed PL-MRRS dual-mode strategy. The linear relationship between the HIgG concentration and the intensity of 707 nm PL peaks/300 cm^{-1} MRRS peaks under the excitation of 488 nm laser was established. The limit of detection was 0.93 fg mL^{-1} for PL and 1.10 fg mL^{-1} for MRRS. In comparison with previous IgG detection methods, the proposed method exhibited prominent advantages in detection sensitivity and working range with good stability and repeatability. An internal self-calibration was realized which ensured the accuracy and reliability of detection results. Both results of specificity experiments and serum sample analysis further confirmed the feasibility of the designed immunoassay strategy in practical serological detection.

Introduction

The outbreak of major diseases and public health emergencies has seriously threatened the public health, economy development, and society stability. As the most recent example, the terrible influence of coronavirus disease 2019 (COVID-19) is still ongoing [1, 2]. The variation of antigen level plays a pivotal role in the judgment of disease progression and evaluation of treatment effect [2–5]. Human IgG (HIgG), as the main component of serum protein, is the main force against viruses and important biomarker of various

Hongyi Li and Xiaokun Wen contributed equally to this work.

✉ Huiying Zhao
zhaohuiying163@163.com

✉ Xia Hong
xiahong@nenu.edu.cn

[1] Key Laboratory of UV-Emitting Materials and Technology (Northeast Normal University), Ministry of Education, Changchun 130024, People's Republic of China

[2] Department of Geriatrics, First Hospital of Jilin University, Changchun 130021, People's Republic of China

autoimmune diseases. Its detection is thus of great significance for the early diagnosis, mass screening, and prognosis monitoring [6–8].

The optical methods, such as colorimetric and photoluminescent (PL) strategies, are the mainstream in biodetection [9, 10]. Although the excellent performances like bare eye identification and high sensitivity have been well obtained, the single-mode strategies based on the single optical signal are usually challenged by accuracy due to the susceptibility to the external interferences [11, 12]. Combining two signals as the dual-mode detection strategy attracts much focus on account of the internal verification [13–16]. The dual-mode methods including PL/surface-enhanced Raman scattering (SERS) [17], colorimetry/PL [18], and colorimetry/SERS [19] methods have been developed for HIgG detection. However, those methods integrate two or more functional materials by multifarious steps to obtain the dual signals, which may affect the uniformity or stability of the signals and limit the reproducibility of detection [11]. Hence, to reasonably design and develop the dual-mode nanoprobes with simple structures and components is an important issue.

Semiconductor nanomaterials possess outstanding PL property which makes them superior to design the

nanoprobes [20, 21]. Besides that, some of them have strong electron–phonon interaction which endows them with multiphonon resonant Raman scattering (MRRS) property [22]. Our previous work has confirmed that the MRRS signals are highly stable and can be used in sensitive biodetection [23, 24]. Utilizing the semiconductor nanomaterials as signal carriers of PL and MRRS to design the dual-mode detection strategy may be a solution to simplify the preparation procedures and perform the dual-mode detection with good reproducibility. As a typical II–VI semiconductor material, CdS shows prominent performance in the field of biolabeling and biodetection [25, 26]. More importantly, the bandgap of CdS is 2.42 eV which is in accordance with the energy of 488 nm (2.54 eV) laser. Under the illumination of 488-nm laser, CdS exhibits PL and MRRS properties [27, 28], making it suitable for the design of dual-mode nanoprobe. Nevertheless, there have been no related reports on the PL/MRRS dual-mode strategy using CdS nanoparticles, which may result from that the PL property of CdS is impressive while the MRRS is ignored.

Herein, the CdS nanoparticles with PL and MRRS properties were synthesized by a hydrothermal method. The onerous design and integration of functional materials were avoided and the signal verification capability was remained. The PL and MRRS dual-mode detection strategy was developed for HIgG detection. The feasibility and practical value were illustrated by the serum HIgG detection.

Materials and methods

Chemicals

The chemicals used in experiments are described in the "Supplementary information."

Preparation of CdS nanoparticles

The CdS nanoparticles were prepared according to the reported work [29, 30], and the preparation processes have been put in the Supplementary Information.

Preparation of PL-MRRS nanoprobes

The N-(3-dimethylaminopropyl)-N′-ethylcarbodiimide hydrochloride/N-hydroxysulfosuccinimide sodium salt (EDC/NHS) crosslinking method was used to couple CdS nanoparticles with the antibodies. The ultrasonically redispersed CdS morpholine ethanesulfonic acid (MES) dispersion (1 mL, 80 μg mL^{-1}) was mixed with 0.5 mL EDC/NHS (0.1 M/0.02 M) MES solution (pH = 5.6, 0.05 M) and shaken at 25 °C for 30 min. Subsequently, the dispersion was incubated with goat anti-human IgG (40 μg mL^{-1}, 1 mL) at

37 °C for 1 h. Bovine serum albumin (BSA, 100 μg mL^{-1}, 40 μL) was added, and the mixture was further incubated at 37 °C for 30 min to block unbound sites. The product was centrifuged (6000 rpm, 5 min) for three times and then dispersed in 1 mL deionized water.

Construction of the immunoassay protocol

The immunoassay strategy is illustrated in Fig. 1. The nanoprobes were incubated with HIgG at different concentrations using a shaker at 37 °C for 1 h. The blank control samples were obtained without adding HIgG in the preparation process. Sequentially, the complexes were centrifuged and washed with phosphate buffer saline (PBS) for three times and redispersed into 1 mL PBS. The gold-coated silicon wafers were soaked in thioctic acid ethanol solution (10 mg mL^{-1}) for 6 h, rinsed with ethanol and blown dry. Then, they were immersed in EDC/NHS MES solution for 30 min, washed with deionized water and blown-dried. Finally, the substrates were soaked in goat anti-human IgG (20 μg mL^{-1}), incubated at 37 °C for 1 h and soaked in BSA (100 μg mL^{-1}) for 20 min to block the remaining binding sites.

The substrates were immersed in the nanoprobe/HIgG complex dispersion and the mixture was shaken at 37 °C for 1 h, washed with deionized water and blow-dried. The final substrates were stored at 4 °C in dark conditions before the PL and MRRS spectral tests.

Evaluation of selectivity and specificity

A number of blood disruptors including HIgA, HIgM, uric acid (UA), glucose (GLU), and lysozyme (LYS) were used to evaluate the selectivity and specificity of as-proposed immunoassay strategy for HIgG detection. These disruptors (each of 10 μg mL^{-1}) were in place of or mixed with analyte HIgG (100 pg mL^{-1}) during immunoassay.

Detection of HIgG in serum samples

HIgG solution was replaced with serum samples for testing to verify the practical potential of as-proposed detection strategy. Serum samples were firstly analyzed using commercial ELISA kits (Shanghai Fanke Industrial Co., Ltd) to detect the HIgG content. Then, they were diluted to obtain following concentrations: 10 fg mL^{-1}, 50 fg mL^{-1}, 10 pg mL^{-1}, 50 pg mL^{-1}, and 50 ng mL^{-1}. The other processes of the immunoassay protocol constructing were the same. The serum sample analysis was conducted under the guidance of the Ethics Committee of Northeast Normal University.

Fig. 1 Schematic diagram of the proposed immunoassay strategy
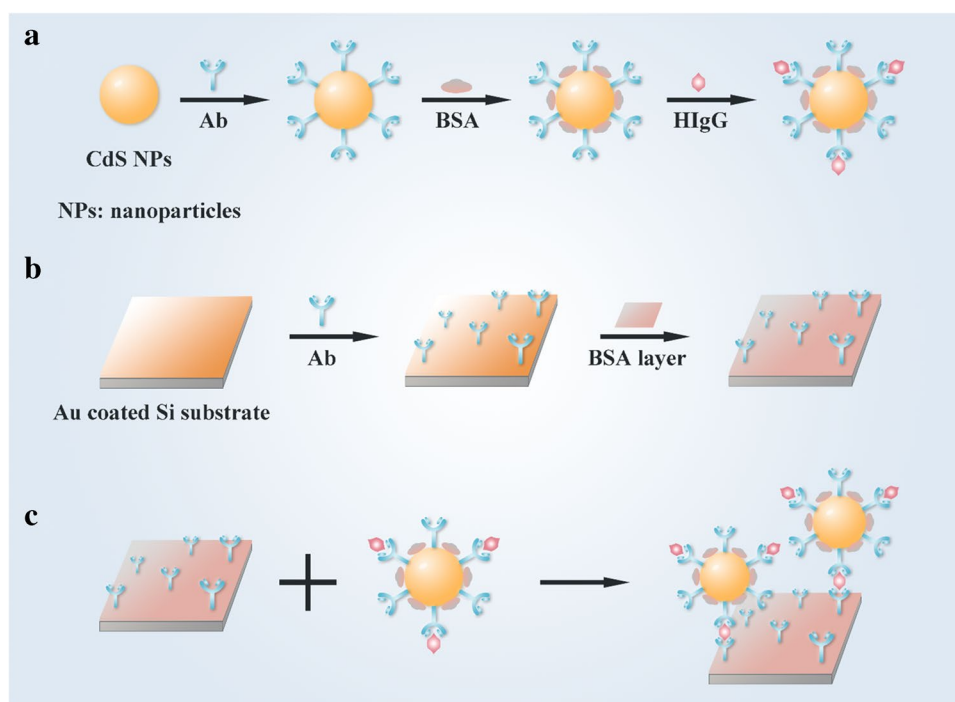
Characterization

The characterization information is described in the "Supplementary information."

Results and discussion

Characterization of CdS nanoparticles

The structure and morphology of CdS nanoparticles prepared by the hydrothermal method were characterized by XRD and TEM. As shown in Fig. 2a, the characteristic peaks of as-prepared samples at 26.5°, 44.0°, 52.1°, 64.0°, 70.4°, and 72.8° corresponded to (111), (220), (311), (400), (331), and (420) crystal planes of cubic sphalerite CdS (JCPDS 10–0454), respectively. It indicates the successful preparation of CdS. The TEM image of CdS nanoparticles is shown in Fig. 2b. It can be seen that the particle size was about 7.2 ± 0.6 nm.

Properties of CdS nanoprobes

CdS nanoprobes were obtained by coupling goat anti-human IgG to CdS nanoparticles via the EDC/NHS crosslinking method. The PL and MRRS properties of CdS nanoprobes were verified by using a 488-nm laser as the excitation light source. The PL spectrum of nanoprobes is shown in Fig. 2c. A weak emission peak centered at 526 nm and a relatively strong one at 707 nm can be observed. Under the irradiation of 488-nm laser, four-order longitudinal optical (LO) phonon scattering signals which arise from the intrinsic electron–phonon coupling were observed at 300 cm^{-1}, 601 cm^{-1}, 902 cm^{-1}, and 1203 cm^{-1}, respectively (Fig. 2d). The equal peak intervals between each LO line were easy to be recognized. The strongest PL peaks at 707 nm and MRRS peaks at 300 cm^{-1} were hence taken as the quantification signals. These results validated the superior PL and MRRS performances of nanoprobes, which provided a crucial prerequisite for the construction of PL-MRRS dual-mode immunoassay strategy.

Optimization of immunoassay conditions

In order to achieve the superior immunoassay, the key experimental parameters including the nanoprobe concentration, incubation time of nanoprobes with analytes, the incubation temperature and time of nanoprobes/analytes mixture with substrates were optimized. As seen in Fig. S1, the optimal condition for dual-mode detection can be set at 21.5 µg mL^{-1}, 60 min, 37 °C, and 60 min.

Assay performance of the proposed dual-mode immunoassay strategy

Under the optimal experimental conditions, the assay performance of as-proposed dual-mode immunoassay strategy was evaluated by using HIgG as the target. The PL and MRRS dual-readout signals were collected on the same apparatus (a Raman spectrometer with 488-nm laser),

Fig. 2 **a** XRD pattern and **b** TEM image of CdS nanoparticles. **c** PL and **d** MRRS spectra of CdS nanoprobes under the illumination of the 488-nm laser
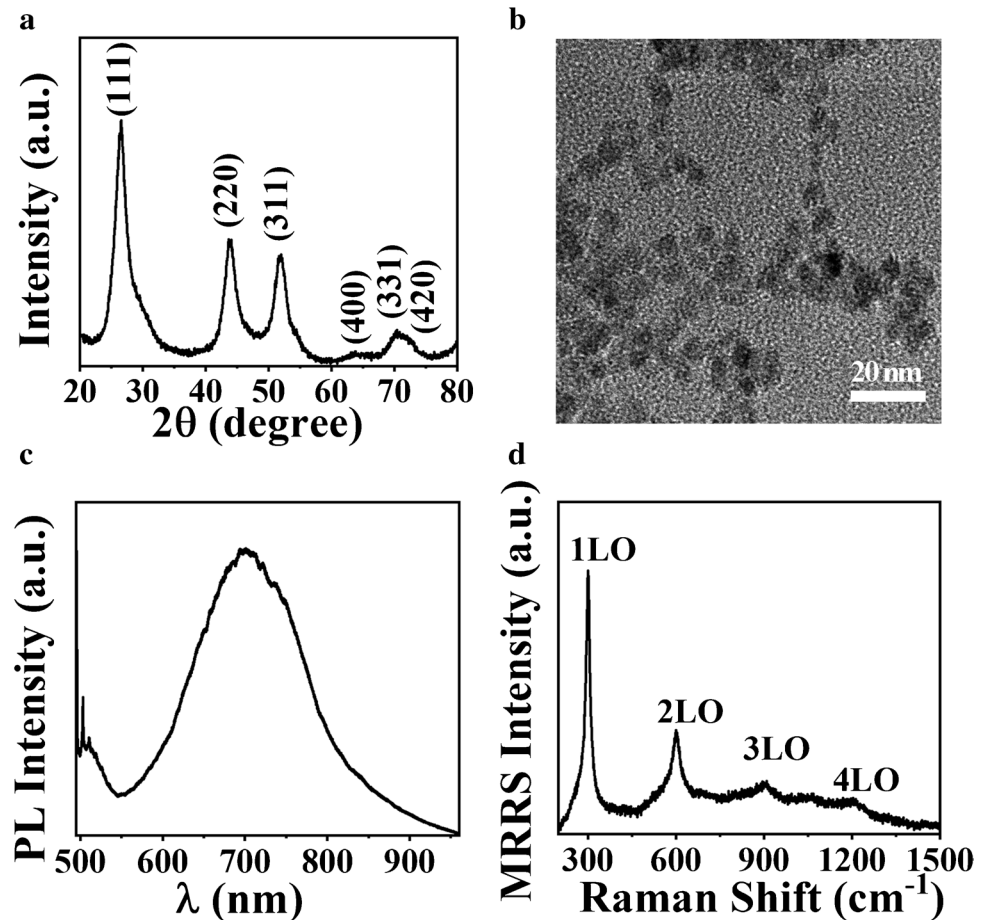
which is in favor of improving the cost efficiency and convenience for the comparison between diverse modes. As shown in Fig. 3a, the PL peak intensity at 707 nm gradually increased with the increase of HIgG concentration. The correlation of PL peak intensity with the logarithm of HIgG concentration had excellent linearity from 2 fg mL^{-1} to 100 ng mL^{-1} with a regression equation of $y = 787.75 \mathrm{Log} c_{\mathrm{HIgG}} + 58.17$ ($R^2 = 0.998$), as shown in Fig. 3b. The limit of detection (LOD) was 0.93 fg mL^{-1} according to the 3σ/slope rule. As the MRRS detection spectra (Fig. 3c) shows, the intensity of MRRS increased with the increase of HIgG concentration. And in Fig. 3d, the linear correlation range of MRRS peak intensity at 300 cm^{-1} with the logarithm of HIgG concentration was from 5 fg mL^{-1} to 100 ng mL^{-1}. The LOD was calculated to be 1.10 fg mL^{-1} while a regression equation of $y = 707.56 \mathrm{Log} c_{\mathrm{HIgG}} + 0.08$ ($R^2 = 0.999$) was obtained. The performance of the proposed dual-mode immunoassay strategy was compared with other reported IgG detection methods, and the results are shown in Table 1. It is not hard to find that the proposed dual-mode immunoassay strategy was comparable to some previous work in both

LOD and detection range. Additionally, the CdS nanoparticles as the single-unit probe with dual signals effectively avoid the multiple-step integration of the signal tags, which may have positive effect on improving the reproducibility of the results [31].

Various interferences are important factors affecting the accuracy of detection results. So as to evaluate the selectivity and specificity of as-proposed dual-mode immunoassay strategy, the experimental investigations were conducted using biological substances commonly found in human body fluids such as HIgA, HIgM, UA, GLU, and LYS as interferences. Each interference was taken to replace or mix with HIgG for the dual-mode immunoassay, and the concentration of each one was set at 10 μg mL^{-1} while that of HIgG was 100 pg mL^{-1}. As shown in Fig. 4, PL and MRRS intensities of the only-interference-contained samples were close to those of the blank control samples. While the interference was mixed with HIgG, PL and MRRS intensities were nearly equal to that of pure HIgG sample. These results revealed the satisfactory selectivity and specificity of the dual-mode immunoassay strategy.

Fig. 3 a PL spectra of the dual-mode immunoassay with HIgG concentrations from 2 fg mL^{-1} to 100 ng mL^{-1}. **b** The linear relationship between PL peak intensity at 707 nm and logarithms of HIgG concentration from 2 fg mL^{-1} to 100 ng mL^{-1}. **c** MRRS spectra of the dual-mode immunoassay with HIgG concentrations from 5 fg mL^{-1} to 100 ng mL^{-1}. **d** The linear relationship between 1LO peak intensity at 300 cm^{-1} and logarithms of HIgG concentration ranging from 5 fg mL^{-1} to 100 ng mL^{-1}. PL and MRRS tests were carried out under a 488-nm laser
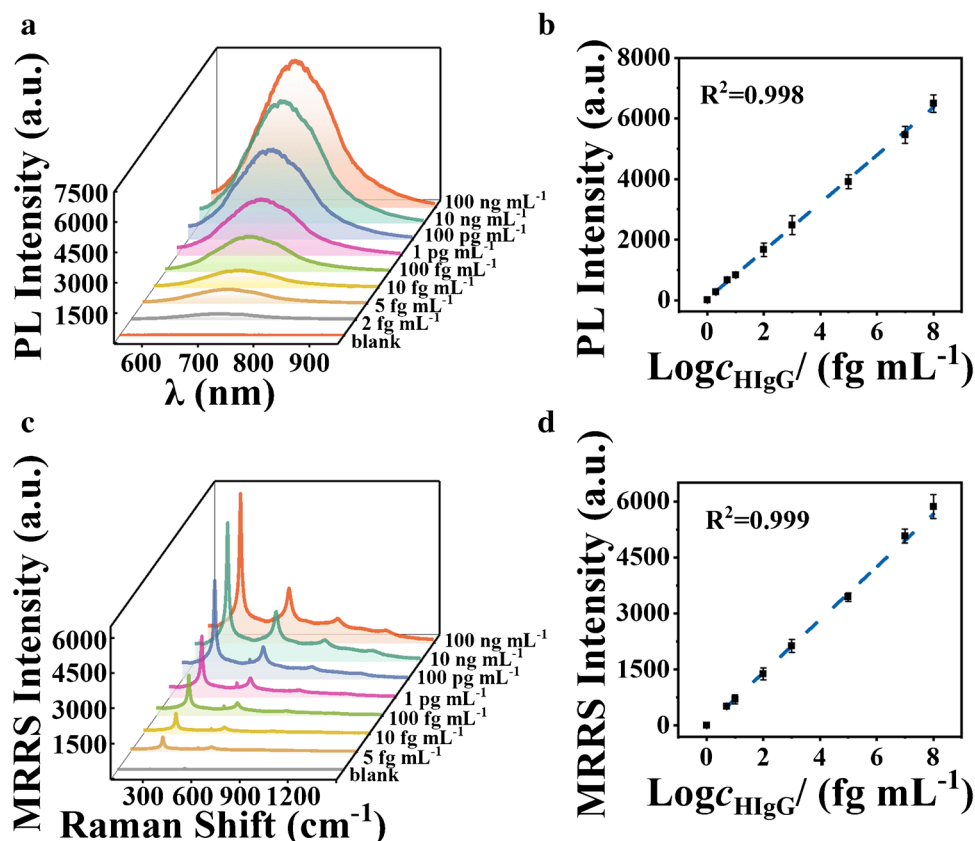

Table 1 Comparison of the strategy in this work with reported IgG detection

Methods[*]	Materials[**]	Linear range	LOD	Ref
FL	GOQDs	1–10^5 pg mL^{-1}	0.21 pg mL^{-1}	[9]
EC	AuNRs/Ferrocene	0.1 fg mL^{-1}–100 ng mL^{-1}	0.1 fg mL^{-1}	[32]
EC	MSNs/CdS	10 pg mL^{-1}–100 ng mL^{-1}	2.9 pg mL^{-1}	[27]
PEC	ZnS-HgS	10 pg mL^{-1}–50 ng mL^{-1}	3.9 pg mL^{-1}	[33]
Colorimetry-CL	LuReGNPs	–	–	[34]
		0.1–100 ng mL^{-1}	33 pg mL^{-1}	
Colorimetry-SERS	4-MBA, Ag@Au Nanoparticles	–	–	[35]
		1 pg mL^{-1}–100 ng mL^{-1}	0.52 pg mL^{-1}	
SERS-FL	Au@Ag, 4-MBA, CdTe	0.1 pg mL^{-1}–1 µg mL^{-1}	0.1 pg mL^{-1}	[18]
		0.1 pg mL^{-1}–1 µg mL^{-1}	–	
PL-MRRS	CdS NPs	2 fg mL^{-1}–100 ng mL^{-1}	0.93 fg mL^{-1}	This work
		5 fg mL^{-1}–100 ng mL^{-1}	1.10 fg mL^{-1}	

[*]*FL* fluorescence; *EC* electrochemistry; *PEC* photoelectrochemistry; *CL* chemiluminescence

[**]*GOQDs* graphene oxide quantum dots; *PEDOT* poly (3,4-ethylenedioxythiophene); *MSNs* mesoporous silica nanospheres; *LuReGNPs* luminol-reduced gold nanoparticles; *4-MBA* 4-mercaptobenzoic acid

Stability and reproducibility assessment

The stability and reproducibility are the decisive criteria for the practical development of as-proposed dual-mode immunoassay strategy. They were evaluated by constructing the detection strategy using 5 parallel systems prepared in the same batch and different batches. Additionally, one detection system with HIgG concentration at 100 pg mL^{-1} was tested after storing for 4 weeks. In each test process, the PL and MRRS detection were repeated 30 times for the calculation of error bars. The detection results of PL and MRRS modes showed no distinct fluctuation as it can be seen in

Fig. 4 **a** PL and **b** MRRS results of selectivity and specificity tests of the dual-mode immunoassay strategy under the irradiation of 488-nm laser, where the 707-nm PL peaks and 300 cm^{-1} MRRS peaks were taken for the quantitation. HIgG concentration was set at 100 pg mL^{-1} and each interference was 10 μg mL^{-1}
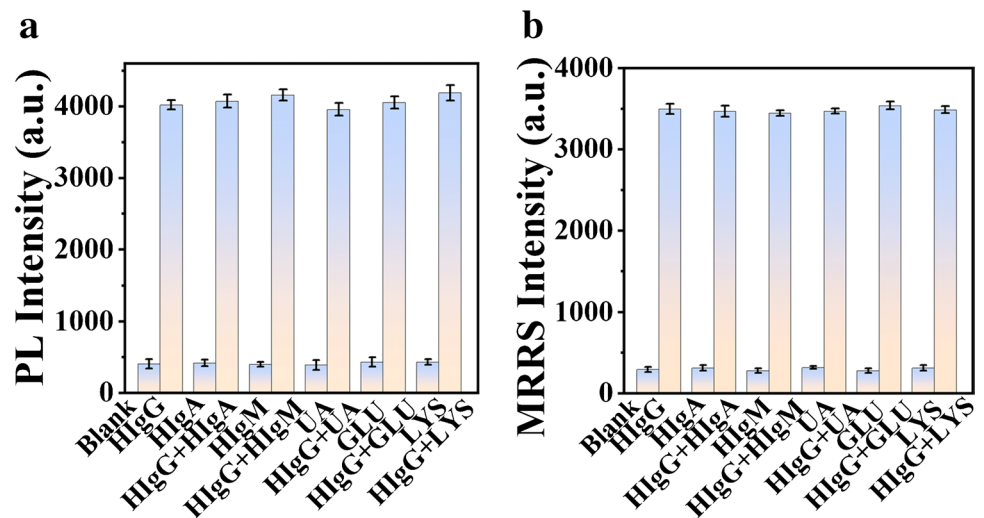
Fig. 5 and Fig. 6. This shows that the strategy had satisfactory stability and reproducibility. These results provided the dual-mode immunoassay strategy a guarantee for further practical research.

Detection of HIgG in human serum samples

Eventually, the serum sample containing a specified concentration of HIgG was used for a recovery experiment to assess the usefulness of the dual-mode immunoassay strategy. The results are summarized in Table 2. The recovery of PL mode ranged from 100 to 101% with relative standard deviation (RSD) in the range of 0.99 to 2.27%. Meanwhile, the recovery of MRRS mode was situated in the range of 99.2 to 101% with the RSD located in the scope of 1.34 to 2.47%. These results confirmed the applicability of the dual-mode immunoassay strategy in ultra-sensitive and high-precision detection of serum HIgG.

Fig. 5 **a** The intensity variation of PL peak at 707 nm obtained for immunoassays with a HIgG concentration of 100 pg mL^{-1} using 5 parallel systems from the same batch and **b** from different batches. **c** The intensity variation of MRRS peak at 300 cm^{-1} obtained for immunoassays with a HIgG concentration of 100 pg mL^{-1} using 5 parallel systems from the same batch, and **d** from different batches. The PL and MRRS tests were carried out under a 488-nm laser
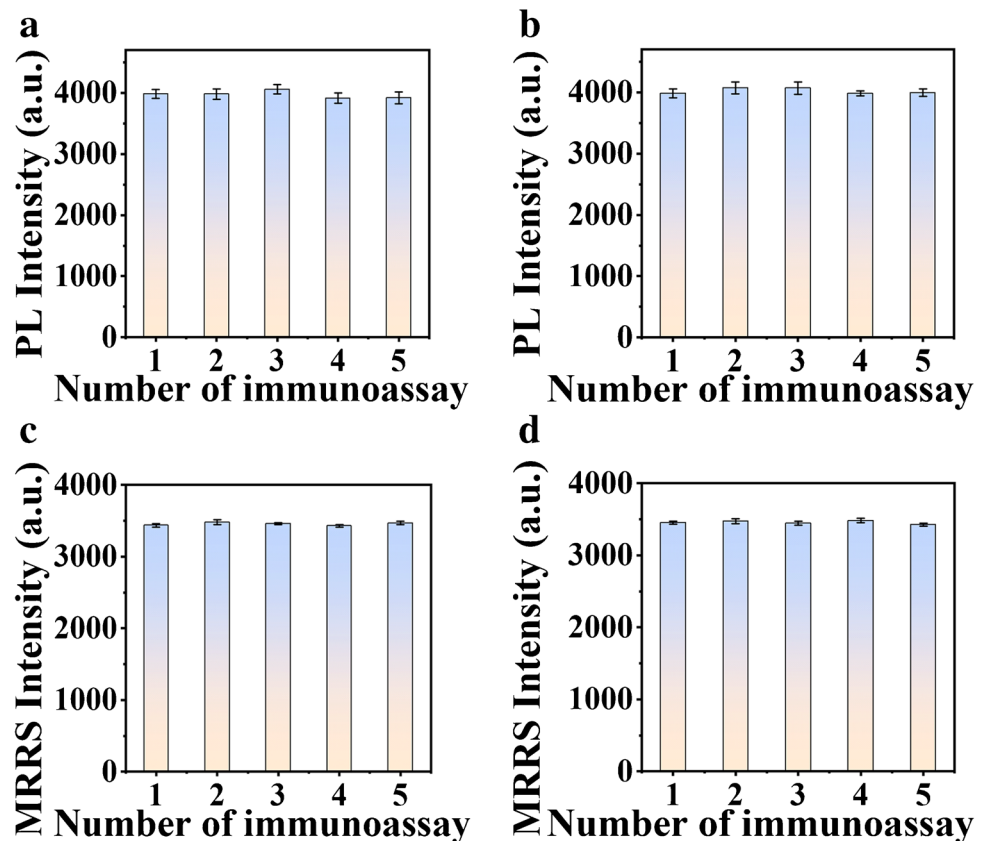
Fig. 6 **a** PL and **b** MRRS results of a detection system with HIgG concentration of 100 pg mL^{-1} before (blue) and after (flesh-colored) 4-week storage. The intensity of PL peaks at 707 nm and MRRS peaks at 300 cm^{-1} were obtained under the irradiation of 488-nm laser
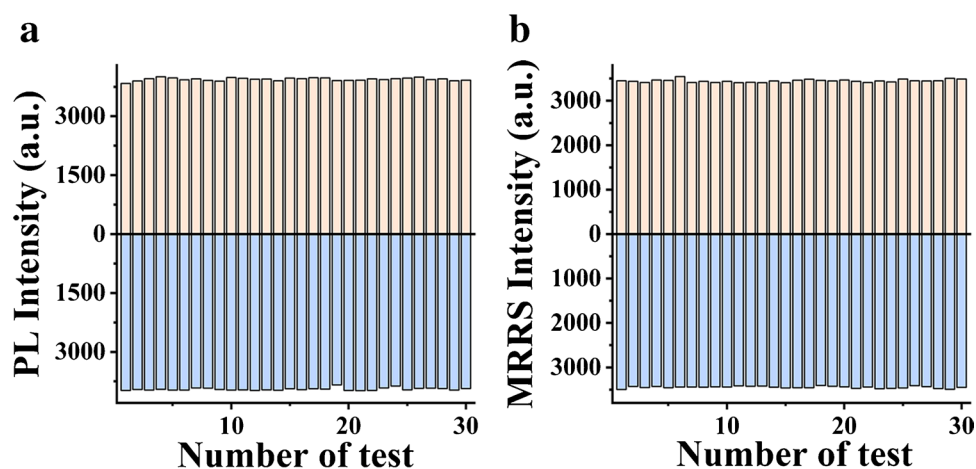

Table 2 PL and MRRS detection results of HIgG in serum samples ($n=5$)

HIgG concentration	Detection result		RSD (%)		Recovery (%)	
	PL	MRRS	PL	MRRS	PL	MRRS
10 fg mL^{-1}	10.1±0.2 fg mL^{-1}	10.0±0.1 fg mL^{-1}	2.24	1.50	101	100
50 fg mL^{-1}	50.3±1.1 fg mL^{-1}	50.3±0.9 fg mL^{-1}	2.27	1.75	101	101
10 pg mL^{-1}	10.0±0.1 pg mL^{-1}	10.0±0.2 pg mL^{-1}	0.99	1.98	100	100
50 pg mL^{-1}	50.1±0.9 pg mL^{-1}	49.6±0.7 pg mL^{-1}	1.74	1.34	100	99.2
50 ng mL^{-1}	50.1±0.8 ng mL^{-1}	49.6±1.2 ng mL^{-1}	1.67	2.47	100	99.2

The consistency between the two modes of dual-mode immunoassay strategy is the key to realize internal self-calibration. The consistency of this strategy was verified by comparing the PL and MRRS results of serum samples. As shown in Fig. S2, the detection results of PL and MRRS showed a good linear relationship with a linear regression equation of $y = 0.999x + 0.001$, which confirmed the excellent detection consistency of the two modes.

Although the dual-mode strategy exhibited excellent performances in both LOD and detection range, there are still some room for improvement. If the gold-coated silicon wafers used in the study can be replaced with other substrates such as the paper-based substrates for point-of-care test (POCT), the cost may be lowered. Additionally, the incubation time of nanoprobe/analyte with the substrates still needs to be shortened. The abovementioned questions should be well solved for the future development.

Conclusions

In conclusion, the CdS nanoparticles were prepared by a hydrothermal method and designed as the dual-signal nanoprobes for the HIgG detection. The combination and complementation of PL and MRRS signals endowed the designed dual-mode immunoassay strategy with ultra-sensitive, wide-range, and high-accuracy specific detection capability. The LOD of PL mode was 0.93 fg mL^{-1} and MRRS mode was 1.10 fg mL^{-1}. The dual-mode immunoassay strategy can be extended to other biomolecule detection by replacing the corresponding antibodies. Nevertheless, there is still distances to the clinical application, such as the exploitation of corresponding kits, the popularization of PL-MRRS spectrometers, and the development of portable equipment.

Declarations

Conflict of interest The authors declare no competing interests.

References

1. Taleghani N, Taghipour F (2021) Diagnosis of COVID-19 for controlling the pandemic: a review of the state-of-the-art. Biosens

Bioelectron 174:112830. https://doi.org/10.1016/j.bios.2020.112830

2. Ernst E, Wolfe P, Stahura C, Edwards KA (2021) Technical considerations to development of serological tests for SARS-CoV-2. Talanta 224:121883. https://doi.org/10.1016/j.talanta.2020.121883

3. Fu Y, Pan YB, Li ZQ, Li YR (2020) The utility of specific antibodies against SARS-CoV-2 in laboratory diagnosis. Front Microbiol 11:603058. https://doi.org/10.3389/fmicb.2020.603058

4. Xu W, Wang D, Li D, Liu CC (2019) Recent developments of electrochemical and optical biosensors for antibody detection. Int J Mol Sci 21:134. https://doi.org/10.3390/ijms21010134

5. Tan XT, Krel M, Dolgov E, Park S, Li XZ, Wu WS, Sun YL, Zhang J, Khaing Oo MK, Perlin DS, Fan XD (2020) Rapid and quantitative detection of SARS-CoV-2 specific IgG for convalescent serum evaluation. Biosens Bioelectron 169:112572. https://doi.org/10.1016/j.bios.2020.112572

6. Bakhshpour M, Chiodi E, Celebi I, Saylan Y, Unlu NL, Unlu MS, Denizli A (2022) Sensitive and real-time detection of IgG using interferometric reflecting imaging sensor system. Biosens Bioelectron 201:113961. https://doi.org/10.1016/j.bios.2021.113961

7. Yang HH, Zhao XQ, Zhang ZW, Ma PY, Wang XH, Song DQ, Sun Y (2022) Biotin-streptavidin sandwich integrated PDA-ZnO@Au nanocomposite based SPR sensor for hIgG detection. Talanta 246:123496. https://doi.org/10.1016/j.talanta.2022.123496

8. Kevadiya BD, Machhi J, Herskovitz J, Oleynikov MD, Blomberg WR, Bajwa N, Soni D, Das S, Hasan M, Patel M, Senan AM, Gorantla S, McMillan J, Edagwa B, Eisenberg R, Gurumurthy CB, Reid SPM, Punyadeera C, Chang L, Gendelman HE (2021) Diagnostics for SARS-CoV-2 infections. Nat Mater 20:593–605. https://doi.org/10.1038/s41563-020-00906-z

9. Wang CH, Wang C, Qiu JY, Gao JW, Liu H, Zhang Y, Han L (2021) Ultrasensitive, high-throughput, and rapid simultaneous detection of SARS-CoV-2 antigens and IgG/IgM antibodies within 10 min through an immunoassay biochip. Microchim Acta 188:262. https://doi.org/10.1007/s00604-021-04896-w

10. Hageneder S, Jungbluth V, Soldo R, Petri C, Pertiller M, Kreivi M, Weinhausel A, Jonas U, Dostalek J (2021) Responsive hydrogel binding matrix for dual signal amplification in fluorescence affinity biosensors and peptide microarrays. ACS Appl Mater Interfaces 13:27645–27655. https://doi.org/10.1021/acsami.1c05950

11. Zhou YF, Huang XL, Hu XY, Tong WP, Leng YK, Xiong YH (2021) Recent advances in colorimetry/fluorimetry-based dual-modal sensing technologies. Biosens Bioelectron 190:113386. https://doi.org/10.1016/j.bios.2021.113386

12. Li YY, Liu L, Liu XJ, Ren Y, Xu K, Zhang N, Sun XJ, Yang XL, Ren X, Wei Q (2020) A dual-mode PCT electrochemical immunosensor with $CuCo_2S_4$ bimetallic sulfides as enhancer. Biosens Bioelectron 163:112280. https://doi.org/10.1016/j.bios.2020.112280

13. Zhang ZH, Li J, Wang XY, Liang AH, Jiang ZL (2019) Aptamer-mediated N/Ce-doped carbon dots as a fluorescent and resonance Rayleigh scattering dual mode probe for arsenic (III). Microchim Acta 186:638. https://doi.org/10.1007/s00604-019-3764-3

14. Wang X, Liao XC, Mei LS, Zhang MM, Chen SY, Qiao XW, Hong CL (2021) An immunosensor using functionalized Cu_2O/Pt NPs as the signal probe for rapid and highly sensitive CEA detection with colorimetry and electrochemistry dual modes. Sens Actuators B Chem 341:130032. https://doi.org/10.1016/j.snb.2021.130032

15. Wei J, Liu SQ, Qileng A, Qin WW, Liu WP, Wang K, Liu YJ (2021) A photoelectrochemical/colorimetric immunosensor for broad-spectrum detection of ochratoxins using bifunctional copper oxide nanoflowers. Sens Actuators B Chem 330:129380. https://doi.org/10.1016/j.snb.2020.129380

16. Xu ES, Yang HT, Li P, Wang Z, Liu Y, Wei W, Liu SQ (2021) Dual-mode detection of PARP-1 by fluorescence and chemiluminescence. Sens Actuators B Chem 330:129288. https://doi.org/10.1016/j.snb.2020.129288

17. Zong SF, Wang ZY, Zhang RH, Wang CL, Xu SH, Cui YP (2013) A multiplex and straightforward aqueous phase immunoassay protocol through the combination of SERS-fluorescence dual mode nanoprobes and magnetic nanobeads. Biosens Bioelectron 41:745–751. https://doi.org/10.1016/j.bios.2012.09.057

18. Wang CW, Yang XS, Gu B, Liu HF, Zhou ZH, Shi LL, Cheng XD, Wang SQ (2020) Sensitive and simultaneous detection of SARS-CoV-2-Specific IgM/IgG using lateral flow immunoassay based on dual-mode quantum dot nanobeads. Anal Chem 92:15542–15549. https://doi.org/10.1021/acs.analchem.0c03484

19. Liu HF, Dai EH, Xiao R, Zhou ZH, Zhang ML, Bai ZK, Shao Y, Qi KZ, Tu J, Wang CW, Wang SQ (2021) Development of a SERS-based lateral flow immunoassay for rapid and ultra-sensitive detection of anti-SARS-CoV-2 IgM/IgG in clinical samples. Sens Actuators B Chem 329:129196. https://doi.org/10.1016/j.snb.2020.129196

20. Cardoso Dos Santos M, Algar WR, Medintz IL, Hildebrandt N (2020) Quantum dots for Förster resonance energy transfer (FRET). Trends Analyt Chem 125:115819. https://doi.org/10.1016/j.trac.2020.115819

21. Castro RC, Saraiva MLMFS, Santos JLM, Ribeiro DSM (2021) Multiplexed detection using quantum dots as photoluminescent sensing elements or optical labels. Coord Chem Rev 448:214181. https://doi.org/10.1016/j.ccr.2021.214181

22. Arora AK, Rajalakshmi M, Ravindran TR, Sivasubramanian V (2007) Raman spectroscopy of optical phonon confinement in nanostructured materials. J Raman Spectrosc 38:604–617. https://doi.org/10.1002/jrs.1684

23. Wang KX, Xing XT, Ding YD, Guo WQ, Hong X, Zhao HY (2020) Resonance Raman scattering-infrared absorption dual-mode immunosensing for carcinoembryonic antigen based on $ZnO@SiO_2$ nanocomposites. Biosens Bioelectron 150:111870. https://doi.org/10.1016/j.bios.2019.111870

24. Wen XK, Ding YD, Li ZP, Wang KX, Zhao HY, Hong X (2022) A bimodal strategy for highly sensitive and accurate miRNA-21 detection based on photoluminescence and multi-phonon resonant Raman scattering properties of ZnTe nanoparticles. Sens Actuators B Chem 363:131821. https://doi.org/10.1016/j.snb.2022.131821

25. Wang J, Han HY, Jiang XC, Huang L, Chen LN, Li N (2012) Quantum dot-based near-infrared electrochemiluminescent immunosensor with gold nanoparticle-graphene nanosheet hybrids and silica nanospheres double-assisted signal amplification. Anal Chem 84:4893–4899. https://doi.org/10.1021/ac300498v

26. Guo P, Wang Y, Chen ZC, Jin TQ, Fu L, Lin CT, Lai GS (2018) Voltammetric immunoassay of human IgG based on the release of cadmium (II) from CdS nanocrystals deposited on mesoporous silica nanospheres. Microchim Acta 186:15. https://doi.org/10.1007/s00604-018-3142-6

27. Xu XL, Zhao YY, Sie EJ, Lu YH, Liu B, Ekahana SA, Ju X, Jiang QK, Wang JB, Sun HD, Sum TC, Huan CH, Feng YP, Xiong QH (2011) Dynamics of bound exciton complexes in CdS nanobelts. ACS Nano 5:3660–3669. https://doi.org/10.1021/nn2008832

28. Baranov AV, Inoue K, Toba K, Yamanaka A, Petrov VV, Fedorov AV (1996) Resonant hyper-Raman and second-harmonic scattering in a CdS quantum-dot system. Phys Rev B 53:1721–1724. https://doi.org/10.1103/physrevb.53.r1721

29. Shi GF, Cao JT, Zhang JJ, Liu YM, Chen YH, Ren SW (2015) An electrochemiluminescence aptasensor based on flowerlike CdS–MoS_2 composites and DNA zyme for detection of immunoglobulin E. Sens Actuators B Chem 220:340–346. https://doi.org/10.1016/j.snb.2015.05.079

30. Zhao JZ, Yang H, Li Y, Lu K (2019) Photocatalytic activity of CdS nanoparticles enhanced by the interaction between piezotronic effect and phase junction. J Alloys Compd 815:152494. https://doi.org/10.1016/j.jallcom.2019.152494

31. Jin H, Sun ZJ, Sun YJ, Gui RJ (2020) Dual-signal ratiometric platforms: Construction principles and electrochemical biosensing applications at the live cell and small animal levels. Trends Anal Chem 134:116124. https://doi.org/10.1016/j.trac.2020.116124

32. Zhang B, Liu BQ, Tang DP, Niessner R, Chen GN, Knopp D (2012) DNA-based hybridization chain reaction for amplified bioelectronic signal and ultrasensitive detection of proteins. Anal Chem 84:5392–5399. https://doi.org/10.1021/ac3009065

33. Shi HH, Li L, Zhang LN, Yu JH (2021) In situ controllable heterojunction conversion strategy driven by oriented paper-based fluid transfer for human immunoglobulin G detection. Microchim Acta 188:373. https://doi.org/10.1007/s00604-021-05017-3

34. Ouyang H, Wang MY, Wang WW, Fu ZF (2018) Colorimetric/chemiluminescent immunochromatographic test strip by using luminol-reduced gold nanoparticles as dual-response probes. Sens Actuators B Chem 266:318–322. https://doi.org/10.1016/j.snb.2018.03.115

35. Liang PH, Guo Q, Zhao TY, Wen CY, Tian ZY, Shang YX, Xing JY, Jiang YZ, Zeng JB (2022) Ag nanoparticles with ultrathin Au shell-based lateral flow immunoassay for colorimetric and SERS dual-mode detection of SARS-CoV-2 IgG. Anal Chem 94:8466–8473. https://doi.org/10.1021/acs.analchem.2c01286